Size-Dependent Nucleation in Crystal Phase Transition from Machine Learning Metadynamics

Pedro A. Santos-Florez,[1] Howard Yanxon,[2] Byungkyun Kang,[1] Yansun Yao,[3,*] and Qiang Zhu[1,†]
[1]Department of Physics and Astronomy, University of Nevada, Las Vegas, Nevada 89154, USA
[2]X-Ray Science Division, Argonne National Laboratory, Lemont, Illinois 60439, USA
[3]Department of Physics and Engineering Physics, University of Saskatchewan, Saskatoon, Saskatchewan, S7N 5E2, Canada

(Received 1 June 2022; revised 5 August 2022; accepted 11 September 2022; published 28 October 2022)

In this Letter, we present a framework that combines machine learning potential (MLP) and metadynamics to investigate solid-solid phase transition. Based on the spectral descriptors and neural networks regression, we develop a scalable MLP model to warrant an accurate interpolation of the energy surface where two phases coexist. Applying it to the simulation of B4–B1 phase transition of GaN under 50 GPa with different model sizes, we observe sequential change of the phase transition mechanism from collective modes to nucleation and growths. When the size is at or below 128 000 atoms, the nucleation and growth appear to follow a preferred direction. At larger sizes, the nuclei occur at multiple sites simultaneously and grow to microstructures by passing the critical size. The observed change of the atomistic mechanism manifests the importance of statistical sampling with large system size in phase transition modeling.

DOI: 10.1103/PhysRevLett.129.185701

Solid-solid phase transitions driven by pressure or temperature are important for our understanding of crystal formation in geological processes, as well as the materials' manufacturing (e.g., steel making, synthesis of ceramics, or creating diamond from carbon under high pressure [1]). Despite their ubiquity, however, elucidation of the microscopic mechanism of solid-solid phase transitions is significantly challenging, due to the need of *in situ* high-resolution imaging technology under extreme conditions. Therefore, computational studies have been devoted to investigate solid-solid phase transitions and provide insights to the microscopic mechanism. Atomistic simulations based on molecular dynamics (MD) can trace atomic motions in phase transitions, but their effectiveness is hindered by the length and timescales allowed for these simulations [2]. Commonly used *ab initio* simulations are restricted up to a few thousands of atoms [3] and therefore can only mimic energy barrier crossing via concerted motion of atoms. Most solid-solid phase transitions are thermodynamically first order and initialized by nucleation that may proceed through intermediate states. When a nucleus grows in a crystal, free energy is gained in the core but penalized at the interface. The competition between these two contributions results in a nucleation barrier, which the system must overcome for the nucleus to grow to a critical size, leading to a cascade of bulk changes [4,5]. The primary difficulty in simulating nucleation and grain growths is the requirement of a very large system size to enable statistical sampling and avoid nuclei interacting with their periodic images. A realistic material simulation must reach beyond collective atomic motions to enable such nucleation dynamics, while at the same time maintaining a truthful description of the material, as opposed to model simulations [6,7].

Notable progress has been made in simulating phase transition from metadynamics [8,9] over the years. This method is designed to overcome large energy barriers through positively biased MD. In metadynamics, the free energy (G) is described by a number of collective variables (CVs, denoted as $\boldsymbol{s}$). To drive the system out of an energy well, G is continuously modified by filling Gaussian potentials that discourage the revisit of already explored phase space. At time step t, the total free energy is expressed as [9]

$$G^t(\boldsymbol{s}) = G(\boldsymbol{s}) + \sum_{t'<t} W e^{-|\boldsymbol{s}-\boldsymbol{s}^{t'}|^2/2\delta s^2}, \tag{1}$$

where W and δs are the height and width of the Gaussian. At each metastep, $\boldsymbol{s}$ follows

$$\boldsymbol{s}^{t+1} = \boldsymbol{s}^t + \delta s \frac{\boldsymbol{F}^t}{|\boldsymbol{F}^t|}, \tag{2}$$

and $|\boldsymbol{F}^t| = -\partial G^t/\partial \boldsymbol{s}$.

Metadynamics has been used successfully to study phase transitions in a variety of systems [10–15]. Recently, the simulation has been scaled up with Gaussian process regression (GPR) potential [16] for a B4–B1 phase transition in GaN (up to 4096 atoms) using a scaled lattice matrix as the CVs, where the onset of nucleation is revealed [17]. In another work, metadynamics simulation is carried

out using classical potentials and two CVs, namely, coordination number and volume, which achieves the simulation of B1–B2 transition in NaCl proceeding via nucleation and growth up to 64 000 atoms [18]. These studies adopt either classical or machine learning potentials, providing a compromise between accuracy and system size.

In the present Letter, we focus on providing a scheme for a substantially scaled up simulation of solid-solid phase transitions using machine learning representation of multidimensional free energy surfaces. We developed an efficient method for training neural network (NN) potential [19] on a dataset, including structures, stress tensors, and interatomic forces calculated at density functional theory (DFT) level. We show that the potential is capable of collecting all relevant information needed for solid-solid phase transitions and for describing the nucleation dynamics. The metadynamics scheme is implemented to allow all degrees of freedom of the supercell to evolve during the simulation, thus enabling a realistic path selection. The applicability of this method is demonstrated using a classic example, the B4–B1 phase transition in GaN, consisting of a simulation box with size up to half a million atoms under high pressure. GaN is a wide band gap semiconductor of technological importance. Multiple transition paths were proposed [20,21], exhibiting the complexity of its transition. Our simulation reveals the bulk phase transition through nucleation and growths and a system-size-dependent crossover from directional nucleation of a single cluster to homogeneous nucleation of multiple clusters.

In the past decade, machine learning methods have been widely applied to resolve the dilemma of compromising between accuracy and cost [22]. Machine learning potentials (MLPs) are trained by minimizing the cost function to attune the model to deliberately describe the *ab initio* data. Among many different MLP models, both NN and GPR techniques are becoming popular in the materials modeling community. Compared to GPR, the NN technique is more suitable for large scale simulation because of its better scalability. Recently, we have developed the NN version of spectral neighbor analysis potential (NN-SNAP) [23–26] based on the bispectrum coefficient descriptors [16,27] and implemented them to the LAMMPS software [28] with the option of mixing with other empirical models [29]. To train an accurate NN-SNAP model for describing the GaN's B4–B1 transition, we start with the existing dataset from a recent work [17] with the VASP code [30] and the Perdew-Burke-Ernzerhof exchange-correlation functional [31]. We apply the trained model to run *NPT* MD simulation for 64 atoms B4–B1 models at different conditions to sample more phase space. The representative MD configurations are collected for single-point DFT calculations (see Fig. S1 and Table S1 in the Supplemental Material [32]) to improve the NN-SNAP model. Finally, we run another similar iteration based on metadynamics simulation of the 32 and 64 atoms models, ensuring that the final model can accurately describe the transition paths between B4 and B1 energy basins on the potential energy surface (PES).

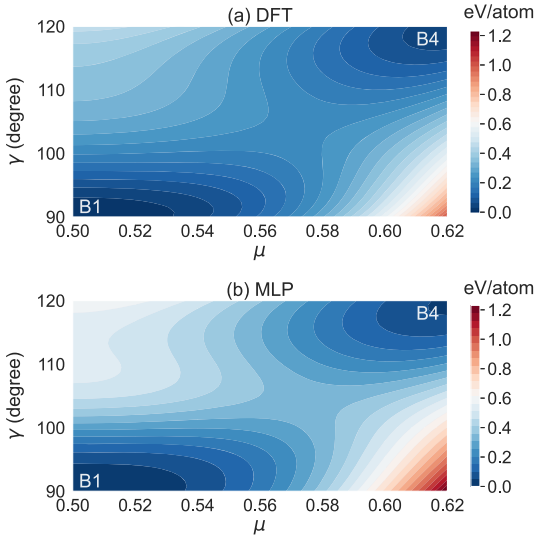

FIG. 1. Comparison of the B4–B1 PES of GaN at 50 GPa computed using (a) DFT and (b) MLP methods.

To check the validity of our MLP, we examined some basic physical quantities with respect to the DFT results. In the past DFT studies [20,21,33], it was found that three key variables describe the B4–B1 transition of GaN, including (1) the spacing μ between Ga/N sublattices changing from 0.5 to 0.62, (2) the basal angle γ decreasing from 120° to 90°, and (3) the c/a ratio reducing from 1.633 to 1.414. Multiple transition paths can be envisioned upon switching the orders of these changes, resulting in different intermediate phases. Following our earlier work [33], we checked the 2D PES of a four atoms GaN system as a function of μ and γ. As shown in Fig. 1, our MLP can well reproduce the DFT's PES, despite some negligible discrepancies at the high-energy regions. Since these data were not part of the dataset used in the training, the agreement in blind predicting PES warrants a good interpretive capability of our MLP, which enables an accurate description of the nucleation region where the two phases coexist. In addition, we checked the densities, elastic properties, and phonon dispersion for both B1 and B4 structures in a wide range of pressure and observed an overall good agreement (see Figs. S2 and S3 in the Supplemental Material [32]).

Furthermore, we perform metadynamics simulations (by using the six-dimensional cell parameters as the CVs) to explore the B4–B1 transition. Figure 2 shows a typical trajectory (enthalpy evolution with metastep) for a system consisting of 128 atoms at 50 GPa. In this simulation, the Gaussian parameters were set as $\delta s = 0.2$ Å and $W = 3000$ GPa Å^3, respectively. Once the evolution reached the B1 phase, we recalculated the enthalpy along the MLP

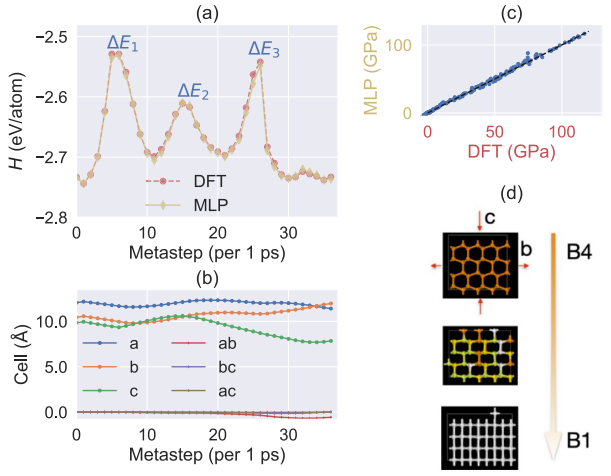

FIG. 2. The metadynamics simulation of 128 atoms GaN's B4–B1 transition. (a) Evolution of enthalpy (H) in MLP-based metadynamics (yellow) simulation. The enthalpies along the trajectory were recomputed with DFT (red) for a comparison. (b) Evolution of CVs along the trajectory. (a, b, c) and (ab, bc, ac) denote uniaxial and shear modes, respectively. (c) Stress tensors from DFT and MLP calculations. (d) Atomistic motions at critical steps, in which atoms in orange and white denote the four-coordinated B4 and six-coordinated B1 environments.

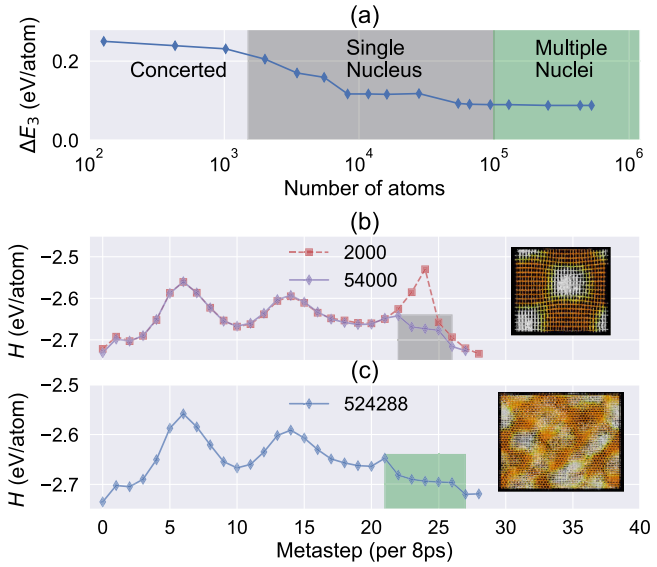

FIG. 3. The size-dependent metadynamics simulations of GaN's B4–B1 transition. (a) Evolution of phase transition barrier (ΔE_3) as a function of system size. (b) and (c) Time evolution of enthalpy (H) during the phase transition for several selected systems. Two representative inset snapshots show directional [in (b)] and homogeneous [in (c)] nucleation mechanisms.

trajectory with DFT. From Fig. 2(a), it is clear that the computed DFT energies nearly overlay with the MLP results. More importantly, the stress tensors, as the driver for the phase change, are well reproduced in MLP [Fig. 2(c)]. The excellent agreements suggest that our MLP trained with smaller systems is applicable to large scale simulations at the accuracy on par with DFT.

According to Fig. 2, the entire simulation can be divided into three stages. Stage (i) corresponds to a simultaneous compression of a, b, and c axes at the first ten metasteps. These changes clearly require a high penalty energy ($\Delta E_1 = 0.204$ eV/atom) and therefore the attempt quickly gives up and the unit cell bounces back. As a consequence of overcompression in (i), stage (ii) acts in an opposite way through expansion. Its penalty energy is lower ($\Delta E_2 = 0.122$ eV/atom) and only the c axis starts to rebound when it reaches the second peak. Afterward, metadynamics starts to explore different evolution and finds a transition path at stage (iii), via simultaneous large compression on c and small expansion on b (while a has minor change). To complete the transition, the system goes through a sharp barrier of ΔE_3 of 0.191 eV/atom. At this system size, the phase transition still undergoes a concerted manner. Figure 2(d) presents the schematic picture of the observed transition mechanism. The large reduction in c results in a decrease of c/a ratio. The increment in b causes the change in basal angle γ. The internal spacing μ is progressively modified through MD equilibrium after the unit cell change in each metastep.

Although we also found several other B4–B1 transition paths in the metadynamics simulation, the results in Fig. 2 provide a relatively simple picture as it can identify a successful path within only a few attempts. Using the same scaled Gaussian parameters, we proceed to investigate the dependence of system size by varying the number of atoms (N).

Table S3 in [32] summarizes the details of all metadynamics simulations in this study. Both ΔE_1 and ΔE_2 quickly converge as the system goes beyond 2000 atoms (see Fig. S4 [32]). They represent two hard modes that cannot initiate the phase transition. However, ΔE_3, corresponding to the barrier of low-energy transition path between B4 and B1, is found to continuously decrease with the system size. Figure 3(a) shows the evolution of ΔE_3 as a function of system size. Up to $N = 1024$, the system undergoes concerted transition in which ΔE_3 steadily drops with increasing system size. The mechanism changes to nucleation in a 2000 atoms system [Fig. 3(a)]. The analysis of metadynamics trajectories (Figs. S5–S7 [32]) shows clear evidence of nucleus formation at the critical stage. The B1 nucleus for $N = 2000$ grows rapidly and completes the entire transition within only one metastep with an energy barrier of 0.215 eV/atom. The nucleation process is seen to be particularly effective in further reducing the barrier in larger systems. The terminal value of the energy barrier is around 0.1 eV/atom when $N = 524\,288$, the largest system attempted in the present study.

Recently, a similar trend was also observed in the study of B1–B2 transition based on a classical potential and two CVs [18]. In that work, the authors suggest that a smaller

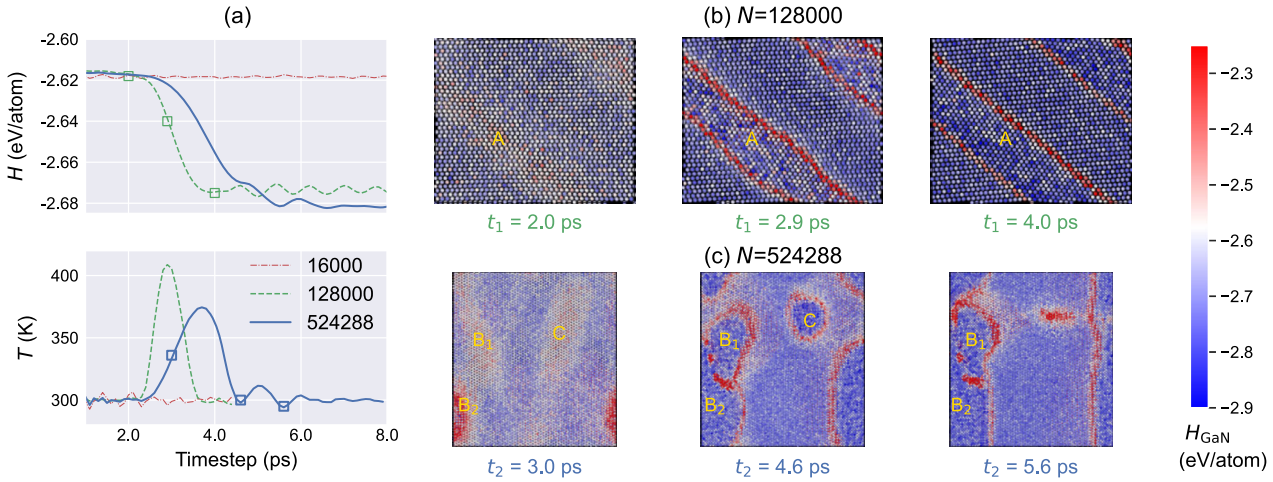

FIG. 4. The size-dependent nucleation process in GaN's B4–B1 transition. (a) Variation of enthalpy and temperature as a function of time for $N = 16\,000$, $128\,000$, and $524\,288$. (b),(c) Selected MD snapshots for $N = 128\,000$ and $524\,288$, respectively. Several representative nucleus sites (**A**, $\mathbf{B}_1$, $\mathbf{B}_2$, **C**) are marked in gold color to guide the eye. To compute H_{GaN}, the atomic volumes are estimated by Voronoi tessellation from OVITO [36].

number of CVs should be used to study nucleation in large systems. However, our simulations, based on the six-dimensional cell parameters [9], are able to produce the same physical picture. This maybe due to an accurate MLP enabling a faithful configuration exploration on the PES. Allowing all degrees of freedom in the system to change enables the simulation to sample more phase space and atomic events. Up to $N = 128\,000$, the nucleus formation and growth is observed to always follow a preferred direction. Nevertheless, simulations with larger sizes suggest more homogeneous nucleation events. Compared to the directional nucleus picture as shown in Fig. 3(b), we find multiple nuclei with different sizes and orientations appearing at the early stage of phase transition [see Fig. 3(c)].

To understand the size dependence of the nucleation mechanism, we focus on analyzing the results of three representative systems ($N = 16\,000$, $128\,000$, and $524\,288$). From each of their metadynamics trajectories, we picked critical metasteps that are around the phase transition window and ran longer NVT MD simulations with both Nosé-Hoover [34] and Langevin [35] thermostats up to 15 ps with the same strain condition. This is to elongate the time window allowed for atomic nucleation in one metastep. As shown in Fig. 4(a), the system size clearly has a marked impact on the phase transition. While there is only an oscillation for $N = 16\,000$, we observe phase transition events for two larger systems shown by the sizable changes in both temperature and enthalpy. For $N = 128\,000$, it has a single transition window between $t_1 = 2.0$ and 4.0 ps. As shown in Fig. 4(b), it first undergoes atomic fluctuation to initiate a nucleus site (marked as **A**). The **A** site then continues to grow along the [110] direction as shown by the expansion of interface regions (colored in red). The critical nucleus, similar to other recent studies [17,18], is a cylindrical volume extending across the periodic boundary. While the system size seems to suppress the development of multiple nuclei, a smaller interface-to-volume ratio favors the formation of a cylindrical nucleus.

However, the trajectory for $N = 524\,288$ exhibits a more complicated picture with three stages. First, multiple nuclei [marked as $\mathbf{B}_1$, $\mathbf{B}_2$, and **C** in Fig. 4(c)] emerge simultaneously until $t_2 = 3.0$ ps, which causes the temperature of the system to rise. Further, these nuclei grow and start to interact with each other, when they get close around $t_2 = 4.5$–5.7 ps. These nuclei are three dimensional in nature; some are not far from spheres. Closer nuclei (i.e., $\mathbf{B}_1$ and $\mathbf{B}_2$) merge into a microstructure and bypass the critical size. The grains reach the largest size at peak temperature, which agrees with the classical theory of nucleation for two competing effects with respect to temperature [37]. After this stage, the number of grains decreases, and the temperature drops accordingly. Some nuclei like **C** stop growing before reaching the critical size and eventually disappear. Similar homogeneous nucleation and microstructure formation have been observed in previous classical simulations with close to a million atoms [38], which manifests the importance of the statistical sampling with large size.

In general, a larger system size with multiple nuclei can reduce the barrier further as compared to the single-nucleus picture. In addition, Fig. S9 [32] lists the evolution of simulated x-ray diffraction patterns for a few representative systems, in which the size-dependent transition paths are revealed. Large system size, consisting of the full information of atomic packing, nuclei, and grain boundaries, can generate a more realistic diffraction pattern, thus allowing for the comparison with experimental measurement to identify the intermediate phases during phase transition from ultrafast loading and dynamic x-ray diffraction measurement [39,40].

In summary, we report the application of MLP in solid-solid phase transition simulations, demonstrated in the B4–B1 transition of GaN. We trained a neural network potential and validated it by a set of benchmark calculations. The potential is effective for describing rare events such as nucleation and growths, which leads to accurate atomistic modeling at a large scale. By varying the system size up to a half million atoms in metadynamics simulation, we observe sequential change of the phase transition mechanism from collective modes to directional nucleation and to homogeneous nucleation at multiple sites. Nowadays, MLPs are being widely applied to study the phase transitions between crystalline [41], amorphous [42], superionic solids [43], and liquids [44–46]. Compared to these works, we are focusing on a small and well-defined piece of PES that is related to the transition between B4 and B1 phases. These restrictions allow us to thoroughly investigate the size impacts only and extend the previous discussion on the size dependence of nucleation from a static geometry model [4] to dynamic simulation at finite temperature. Given the observed size dependence in the model system, it reasonable to speculate that such size effects may also exist in other systems, which in turn may impact the transition mechanisms, as well as the physical quantities (e.g., transition barrier, phase boundary).

This research is sponsored by the U.S. Department of Energy, Office of Science, Office of Basic Energy Sciences, Theoretical Condensed Matter Physics program, DOE Established Program to Stimulate Competitive Research under Award No. DE-SC0021970 and Natural Sciences and Engineering Research Council of Canada (NSERC). The computing resources are provided by XSEDE (TG-DMR180040), National Energy Research Scientific Computing Center (NERSC) and Compute Canada. The authors thank Dr. Aidan Thompson for helpful discussions regarding the implementation of NN-SNAP into the LAMMPS package.

*yansun.yao@usask.ca
†qiang.zhu@unlv.edu

[1] W. F. Smith, *Principles of Materials Science and Engineering* (McGraw-Hill, New York, 1996).
[2] D. Marx and J. Hutter, *Ab Initio Molecular Dynamics: Basic Theory and Advanced Methods* (Cambridge University Press, Cambridge, England, 2009).
[3] S. Scandolo, Proc. Natl. Acad. Sci. U.S.A. **116**, 10204 (2019).
[4] R. Z. Khaliullin, H. Eshet, T. D. Kühne, J. Behler, and M. Parrinello, Nat. Mater. **10**, 693 (2011).
[5] Q. Huang, D. Yu, B. Xu, W. Hu, Y. Ma, Y. Wang, Z. Zhao, B. Wen, J. He, Z. Liu, and Y. Tian, Nature (London) **510**, 250 (2014).
[6] W. Qi, Y. Peng, Y. Han, R. K. Bowles, and M. Dijkstra, Phys. Rev. Lett. **115**, 185701 (2015).
[7] Y. Peng, F. Wang, Z. Wang, A. M. Alsayed, Z. Zhang, A. G. Yodh, and Y. Han, Nat. Mater. **14**, 101 (2015).
[8] A. Laio and M. Parrinello, Proc. Natl. Acad. Sci. U.S.A. **99**, 12562 (2002).
[9] R. Martoňák, A. Laio, and M. Parrinello, Phys. Rev. Lett. **90**, 075503 (2003).
[10] P. Raiteri, R. Martoňák, and M. Parrinello, Angew. Chem., Int. Ed. **44**, 3769 (2005).
[11] J. Behler, R. Martoňák, D. Donadio, and M. Parrinello, Phys. Rev. Lett. **100**, 185501 (2008).
[12] Y. Yao, D. D. Klug, J. Sun, and R. Martoňák, Phys. Rev. Lett. **103**, 055503 (2009).
[13] J. Sun, D. D. Klug, R. Martoňák, J. A. Montoya, M.-S. Lee, S. Scandolo, and E. Tosatti, Proc. Natl. Acad. Sci. U.S.A. **106**, 6077 (2009).
[14] L. Bonati and M. Parrinello, Phys. Rev. Lett. **121**, 265701 (2018).
[15] H. Niu, Y. I. Yang, and M. Parrinello, Phys. Rev. Lett. **122**, 245501 (2019).
[16] A. P. Bartók, M. C. Payne, R. Kondor, and G. Csányi, Phys. Rev. Lett. **104**, 136403 (2010).
[17] Q. Tong, X. Luo, A. A. Adeleke, P. Gao, Y. Xie, H. Liu, Q. Li, Y. Wang, J. Lv, Y. Yao, and Y. Ma, Phys. Rev. B **103**, 054107 (2021).
[18] M. Badin and R. Martoňák, Phys. Rev. Lett. **127**, 105701 (2021).
[19] J. Behler and M. Parrinello, Phys. Rev. Lett. **98**, 146401 (2007).
[20] S. Limpijumnong and W. R. L. Lambrecht, Phys. Rev. Lett. **86**, 91 (2001).
[21] A. M. Saitta and F. Decremps, Phys. Rev. B **70**, 035214 (2004).
[22] J. Behler, Int. J. Quantum Chem. **115**, 1032 (2015).
[23] A. P. Thompson, L. P. Swiler, C. R. Trott, S. M. Foiles, and G. J. Tucker, J. Comput. Phys. **285**, 316 (2015).
[24] H. Yanxon, D. Zagaceta, B. C. Wood, and Q. Zhu, J. Chem. Phys. **153**, 054118 (2020).
[25] D. Zagaceta, H. Yanxon, and Q. Zhu, J. Appl. Phys. **128**, 045113 (2020).
[26] H. Yanxon, D. Zagaceta, B. Tang, D. S. Matteson, and Q. Zhu, Mach. Learn. **2**, 027001 (2020).
[27] A. P. Bartók, R. Kondor, and G. Csányi, Phys. Rev. B **87**, 184115 (2013).
[28] S. Plimpton, J. Comput. Phys. **117**, 1 (1995).
[29] J. F. Ziegler and J. P. Biersack, in *Treatise on Heavy-Ion Science* (Springer, New York, 1985), pp. 93–129.
[30] G. Kresse and J. Furthmüller, Phys. Rev. B **54**, 11169 (1996).
[31] J. P. Perdew, K. Burke, and M. Ernzerhof, Phys. Rev. Lett. **77**, 3865 (1996).
[32] See Supplemental Material at http://link.aps.org/supplemental/10.1103/PhysRevLett.129.185701 for a detailed description of MLP training, metadynamics simulation, energy analysis, and other computational details.
[33] Y. Yao and D. D. Klug, Phys. Rev. B **88**, 014113 (2013).
[34] S. Nosé, J. Chem. Phys. **81**, 511 (1984).
[35] T. Schneider and E. Stoll, Phys. Rev. B **17**, 1302 (1978).
[36] A. Stukowski, Model. Simul. Mater. Sic. Eng. **18**, 015012 (2009).

[37] S. Okita, W. Verestek, S. Sakane, T. Takaki, M. Ohno, and Y. Shibuta, J. Cryst. Growth **474**, 140 (2017).
[38] Y. Shibuta, K. Oguchi, T. Takaki, and M. Ohno, Sci. Rep. **5**, 13534 (2015).
[39] A. Gleason, C. Bolme, H. Lee, B. Nagler, E. Galtier, D. Milathianaki, J. Hawreliak, R. Kraus, J. Eggert, D. Fratanduono *et al.*, Nat. Commun. **6**, 1 (2015).
[40] Y. Y. Zhang, Y. X. Li, D. Fan, N. B. Zhang, J. W. Huang, M. X. Tang, Y. Cai, X. L. Zeng, T. Sun, K. Fezzaa, S. Chen, and S. N. Luo, Phys. Rev. Lett. **127**, 045702 (2021).
[41] R. Jinnouchi, J. Lahnsteiner, F. Karsai, G. Kresse, and M. Bokdam, Phys. Rev. Lett. **122**, 225701 (2019).
[42] V. L. Deringer, N. Bernstein, G. Csányi, C. Ben Mahmoud, M. Ceriotti, M. Wilson, D. A. Drabold, and S. R. Elliott, Nature (London) **589**, 59 (2021).
[43] B. Cheng, M. Bethkenhagen, C. J. Pickard, and S. Hamel, Nat. Phys. **17**, 1228 (2021).
[44] H. Niu, L. Bonati, P. M. Piaggi, and M. Parrinello, Nat. Commun. **11**, 1 (2020).
[45] V. Naden Robinson, H. Zong, G. J. Ackland, G. Woolman, and A. Hermann, Proc. Natl. Acad. Sci. U.S.A. **116**, 10297 (2019).
[46] B. Cheng, G. Mazzola, C. J. Pickard, and M. Ceriotti, Nature (London) **585**, 217 (2020).